

# Dipolarization Events With Inductive, Radial Electric Fields Observed by Van Allen Probes

Hiroshi Matsui<sup>1</sup>, Roy B. Torbert<sup>1</sup>, Harlan E. Spence<sup>1</sup>, Matthew B Cooper<sup>2</sup>, Charles J Farrugia<sup>3</sup>, Matina Gkioulidou<sup>4</sup>, Tyler J. Metivier<sup>1</sup>, and John Wygant<sup>5</sup>

<sup>1</sup>University of New Hampshire

<sup>2</sup>New Jersey Institute of Technology

<sup>3</sup>University of New Hampshire, USA

<sup>4</sup>JHU/APL

<sup>5</sup>University of Minnesota

December 7, 2022

## Abstract

Dipolarization events with inductive, radial electric fields are examined, using Van Allen Probes data between 2013 and 2018. Two cases are studied, followed by statistical analyses. These events were observed between evening and premidnight magnetic local times (MLTs) under moderate geomagnetic activities. Radial electric field variations, azimuthal magnetic field variations, and energetic protons were often observed when horizontal magnetic fields started to decrease in the dip region. Magnetic field lines were stretched with their motion similar to the gradient B/curvature drift velocities of energetic protons. Signs of electric fields changed when horizontal magnetic fields started to increase in the dipolarization front (DF). Electric field variations were correlated with magnetic field ones with  $\sim 90$  deg. phase shift. These observations are mainly interpreted in terms of energetic proton structures drifting toward the probe locations, while being accompanied by standing waves.

# Dipolarization Events With Inductive, Radial Electric Fields Observed by Van Allen Probes

H. Matsui<sup>1</sup>, R. B. Torbert<sup>1</sup>, H. E. Spence<sup>1</sup>, M. B. Cooper<sup>2</sup>, C. J. Farrugia<sup>1</sup>,  
M. Gkioulidou<sup>3</sup>, T. J. Metivier<sup>1</sup>, and J. R. Wygant<sup>4</sup>

<sup>1</sup>Space Science Center, University of New Hampshire, Durham, NH, USA

<sup>2</sup>Center for Solar-Terrestrial Research, New Jersey Institute of Technology, Newark, NJ, USA

<sup>3</sup>The Johns Hopkins University Applied Physics Laboratory, Laurel, MD, USA

<sup>4</sup>School of Physics and Astronomy, University of Minnesota, Minneapolis, MN, USA

## Key Points:

- Dipolarization events with inductive, radial electric fields were observed in the dusk-side with energetic proton increases.
- Magnetic field lines were often stretched with their motion similar to the gradient  $B$ /curvature drift velocities of energetic protons.
- These events could be due to drifting, energetic proton structures and accompany standing wave signatures.

## Abstract

Dipolarization events with inductive, radial electric fields are examined, using Van Allen Probes data between 2013 and 2018. Two cases are studied, followed by statistical analyses. These events were observed between evening and premidnight magnetic local times (MLTs) under moderate geomagnetic activities. Radial electric field variations, azimuthal magnetic field variations, and energetic protons were often observed when horizontal magnetic fields started to decrease in the dip region. Magnetic field lines were stretched with their motion similar to the gradient  $B$ /curvature drift velocities of energetic protons. Signs of electric fields changed when horizontal magnetic fields started to increase in the dipolarization front (DF). Electric field variations were correlated with magnetic field ones with  $\sim 90$  deg. phase shift. These observations are mainly interpreted in terms of energetic proton structures drifting toward the probe locations, while being accompanied by standing waves.

## 1 Introduction

Dipolarization events of geomagnetic fields have often been reported in the nightside magnetosphere since the 1960's (Cummings et al., 1968; McPherron et al., 1973). Geomagnetic fields typically stretched tailward return to the original dipolar shape during these events. They have often been observed during geomagnetically active periods such as substorms. These events have not only been observed around geosynchronous orbit (e.g., Nagai, 1982), but also in the magnetotail (e.g., Nakamura et al., 2002). These events have been thought to originate from magnetotail reconnection and subsequently propagate earthward. Hall electric fields are formed due to different gyroradii between ions and electrons around the dipolarization front (DF) (Runov et al., 2011). There are reviews on this topic (Sergeev et al., 2012; Kepko et al., 2015). These events have also been observed inside geosynchronous orbit, e.g., by Van Allen Probes (Gkioulidou et al., 2015; Liu et al., 2016). Since background geomagnetic parameters are different from those of the magnetotail, characteristics of the dipolarization events in the inner magnetosphere could also be different.

Dipolarization events are often associated with particle injections. A relation to energetic protons was examined by Baker et al. (1979). Birn et al. (1997) showed that ion injections were shifted duskward, while electron injections were shifted dawnward. Gkioulidou et al. (2015) presented a detailed analysis of multiple dipolarization events

48 on a Van Allen Probe B's orbit. There were various spatial scales  $\sim 2 - 5$  h in mag-  
49 netic local time (MLT). Energetic proton fluxes behaved differently depending on energy  
50 during dipolarizations. Liu et al. (2016) demonstrated that half of dipolarization events  
51 inside geosynchronous orbit were observed with energetic particle injections. In these events,  
52 the observed electric fields were larger. Motoba et al. (2021) showed a superposed epoch  
53 analysis of energetic particle injections and dipolarizations. When the energetic proton  
54 fluxes started to increase, the horizontal magnetic field decreased in some cases, which  
55 could be due to a diamagnetic effect. That proton increase was possibly due to reflected  
56 populations at the DF, observed and modeled in the magnetotail (Zhou et al., 2014).

57 There have been reports that ultra low frequency (ULF) waves were observed dur-  
58 ing dipolarization events. These waves could have standing wave signatures (Takahashi  
59 et al., 1988). Kinetic scales could be involved (Chaston et al., 2014). The Poynting flux  
60 may provide energy source for aurora (Ergun et al., 2015). Nightside ground observa-  
61 tions of field line resonances were examined during substorm intensifications (Samson  
62 et al., 1992). These waves were inferred to be kinetic and occur in the dipolelike region  
63 of the magnetosphere, outside the plasmopause. In addition, ULF waves were observed  
64 in the plasmashet boundary layer during a dipolarization event (Tian et al., 2021).

65 We have previously reported a dipolarization event observed by Magnetospheric  
66 Multiscale (MMS) in the inner magnetosphere (Matsui et al., 2016). Energetic ions were  
67 enhanced in the dip region before the start of the dipolarization, which could cause in-  
68 ductive, radial electric fields or standing waves. A limitation of that study was that the  
69 particle measurement was only performed in a high energy range above tens of keV be-  
70 cause low energy particle instruments were not operational. Here we analyze dipolariza-  
71 tion events observed by Van Allen Probes, by which particle measurements were performed  
72 in a wide energy range in the inner magnetosphere (Mauk et al., 2013). We may exam-  
73 ine the relationship between particles and fields in more detail. In addition, plenty of data  
74 are available after the completion of the mission so that a statistical analysis may be made.  
75 The objective of this study is to investigate dipolarization events with inductive, radial  
76 electric fields in terms of their physical properties. Here we show an analysis for two events  
77 and statistical results.

78 This paper is organized as follows. In Section 2, we describe data to be analyzed.  
79 In Section 3, two case studies are presented. Statistical analyses follow in Section 4. Sum-  
80 mary and conclusions are discussed in Section 5.

## 81 2 Data

82 We analyze field and particle data measured by Van Allen Probes (Mauk et al., 2013)  
83 between 2013 and 2018. Van Allen Probes had equatorial orbits with magnetic latitudes  
84 (MLATs) within 20 deg. from the magnetic equator. The perigee was 1.1  $R_E$  of the geo-  
85 centric distance, while the apogee was 5.8  $R_E$  so that observations were performed in  
86 the inner magnetosphere. There were two probes A and B with slightly different orbits  
87 and therefore the interprobe separation was variable. Orbital periods were  $\sim 9$  h.

88 Magnetic fields were measured by Electric and Magnetic Field Instrument Suite  
89 and Integrated Science (EMFISIS) (Kletzing et al., 2013). We use 1-s data. Electric fields  
90 were measured by Electric Field and Waves (EFW) Instruments (Wygant et al., 2013).  
91 32-Hz data are averaged to 1-s resolution for the analysis. We examine high-energy pro-  
92 ton data with energies between 40 and 600 keV, measured by Radiation Belt Storm Probes  
93 Ion Composition Experiment (RBSPICE) (Mitchell et al., 2013). Spin-averaged, 11-s flux  
94 and moment data (Pitch Angle and Pressure TOF x Energy Proton Rates, PAP\_TOFXEH)  
95 are analyzed. High-energy electron fluxes with energies between 30 keV and 4 MeV were  
96 measured by Magnetic Electron Ion Spectrometer (MagEIS) (Blake et al., 2013) with  
97 11-s resolution. This instrument also measured ions with energies between 60-160 keV  
98 and 1.3 MeV, complementing the RBSPICE measurements. Low-energy proton and elec-  
99 tron fluxes with energies between 1-15 eV and 50 keV were measured by Helium, Oxy-  
100 gen, Proton, and Electron (HOPE) Mass Spectrometer (Funsten et al., 2013) nominally  
101 with 22-s resolution. Proton moment data were calculated in the energy range above 30  
102 eV.

103 Geomagnetic activities are monitored by auroral electrojet ( $AE$ ),  $Kp$  (Matzka, Stolle,  
104 et al., 2021), and  $Dst$  indices, while interplanetary parameters are examined by OMNI  
105 data (King & Papitashvili, 2005).

### 3 Event Studies

In this section we show two dipolarization events. Although both events are common in that dipolarization is accompanied by electric field variations and energetic proton injections with similar timing, the details are not necessarily similar. Therefore, we will be able to illustrate these dipolarization events further by showing two events.

#### 3.1 A Dipolarization Event on 19 July 2013

There was a dipolarization event starting at 18:03:58 UT on 19 July 2013, as observed by Van Allen Probe A. The probe was located at  $L=5.5$ , 19.4 MLT, and MLAT=9.5 deg. Note that an event is considered to start as the horizontal magnetic fields in  $VDH$  coordinates, subtracted by modeled magnetic fields  $B_{T89Q}$  by Tsyganenko (1989) during quiet periods ( $Kp=0$ ), start to increase. Here, cylindrical,  $VDH$  coordinates are defined as follows:  $V$  in the outward direction,  $D$  in the eastward direction, and  $H$  in the northward direction along the dipole axis.

This event did not correspond to a geomagnetic storm ( $Dst = -21$  nT). The geomagnetic activity monitored by the  $Kp$  index was moderate with 4<sup>-</sup>. There was some auroral electrojet activity ( $AU = 254$  nT and  $AL = -284$  nT). This could be explained by the OMNI data in which the interplanetary magnetic field (IMF) was quite often southward for the preceding several hours or even longer.

Figure 1 shows an overview plot for magnetic fields and electric fields, followed by energetic proton fluxes and pressure measured by RBSPICE. Magnetic pressure is added in the bottom panel of plasma pressure. Quiet-time, modeled magnetic fields  $B_{T89Q}$  are plotted with measured ones in the top three panels and did not change much during the plotted interval of 10 min because Probe A was close to apogee.

The  $B_H$  component decreased between 18:02:32 and 18:03:58 UT, noted as the dip region, and increased between 18:03:58 and 18:07:40 UT, noted as the DF. The terms, dip and DF, have been used in other studies (e.g., Schmid et al., 2019). Each of the above times are indicated by vertical guidelines. After the dipolarization, the measured magnetic field was closer to the quiet-time, modeled magnetic field, i.e., dipolar configuration. The  $B_D$  component increased in the dip and then decreased in the DF. Since Probe A was located in the northern hemisphere, this variation corresponds to the magnetic

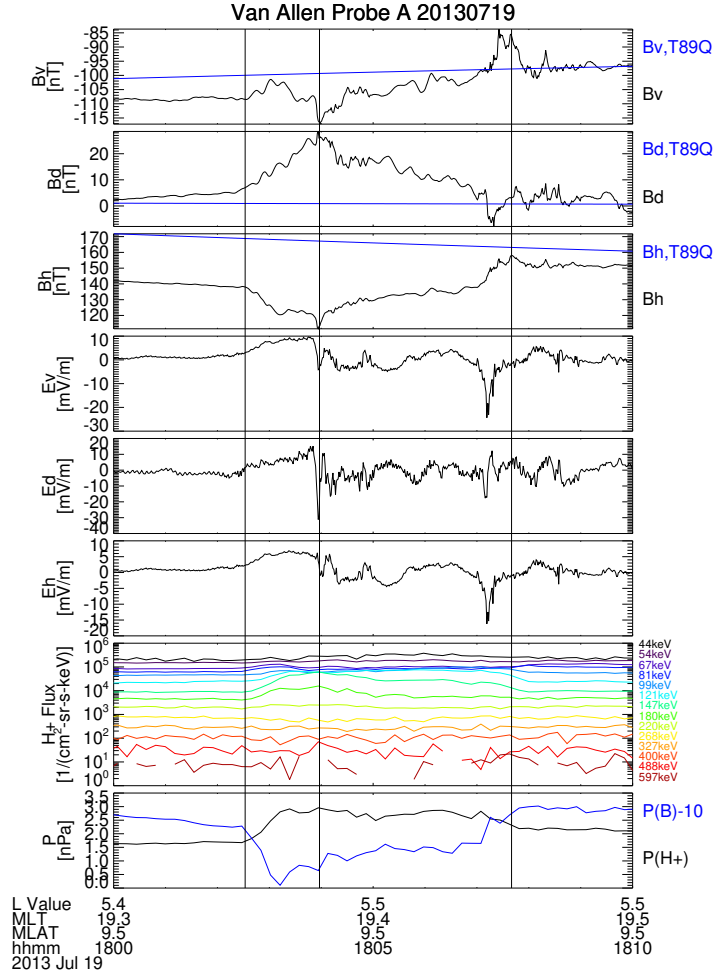


**Figure 1.** An overview plot for a dipolarization event starting at 18:03:58 UT on 19 July 2013, as observed by Van Allen Probe A. Three components of magnetic fields and electric fields in *VDH* coordinates and energetic proton fluxes and pressure measured by RBS-PICE are plotted from top. Modeled magnetic fields  $B_{T89Q}$  are overlaid in the top three panels. Magnetic pressure is added in the bottom panel. Three vertical lines indicate beginning of the dip, ending of the dip or beginning of the DF, and ending of the DF.

136 field line displaced westward in both the dip and DF. This might imply inward current,  
 137 although there is another term related to horizontal magnetic field variations in the az-  
 138 imuthal direction. If static, the inward current indicates westward pressure gradient and  
 139 therefore the field-aligned current (FAC) toward the ionosphere, which could constitute  
 140 Region 2 (R2) current in the evening sector. The  $B_V$  component overall decreased and  
 141 increased in the dip and DF, respectively. Together with the behavior of the  $B_H$  com-

142 ponent, it is inferred that the magnetic field line was stretched outward and then com-  
 143 pressed inward.

144 In the dip region, each electric field component became positive and then approached  
 145 to  $\sim 0$  mV/m, while each magnetic field component increased or decreased to have a  
 146 peak value near the end. We may consider that there was a phase shift  $\sim 90$  degrees  
 147 between electric field and magnetic field variations, taking into account field variations  
 148 afterwards as well. The correspondence between electric and magnetic field variations  
 149 implies electric fields were inductive. Vertical and horizontal electric fields increased by  
 150  $\sim 10$  and  $\sim 5$  mV/m, respectively. Magnetic field lines were stretched westward, con-  
 151 sistent with the  $B_D$  variation mentioned above. Electric field variations were larger than  
 152 typical background convection electric fields of  $< \sim 1$  mV/m. There was also an east-  
 153 ward electric field increase, indicating field lines were moving outward. After that each  
 154 component of electric fields changed its sign with lots of fluctuations in the DF. Mag-  
 155 netic field lines overall moved back eastward and inward.

156 Energetic proton fluxes also increased at  $\sim 45$ – $210$  keV in the dip region. Plasma  
 157 pressure increased by  $1.2$  nPa, while magnetic pressure decreased by  $1.5$  nPa. Total pres-  
 158 sure was approximately conserved. The equatorial gradient  $B$  drift speed of  $75$  keV pro-  
 159 tons under the dipole magnetic field at the  $L$  shell of Probe A,  $5.4$ , is  $\sim 30$  km/s, which  
 160 is similar to the measured, westward component of the  $E \times B$  drift speed  $\sim 50$  km/s.  
 161 Note that the curvature drift speed at the same energy is double of the gradient  $B$  drift  
 162 speed with the same approximation. In the DF, plasma pressure decreased. At this time,  
 163 magnetic pressure increase was larger than plasma pressure decrease.

164 Figure 2 is an overview plot for particle measurements during this dipolarization  
 165 event, together with the  $B_H$  component for reference. When energetic proton fluxes  $> \sim$   
 166  $50$  keV increased, those  $\sim 10$ – $30$  keV decreased. Nonetheless, contribution to the pres-  
 167 sure from the former component was larger (discussed later). Electron fluxes increased  
 168 as the background magnetic field increased. There was no specific injection signature in  
 169 the dip region, contrary to the ions.

### 170 **3.2 A Dipolarization Event on 9 June 2015**

171 Another dipolarization event started at 22:52:07 UT on 9 June 2015. Van Allen Probe  
 172 A was located at  $L = 6.0$ ,  $19.3$  MLT, and MLAT= $11.1$  deg. Some auroral electrojet

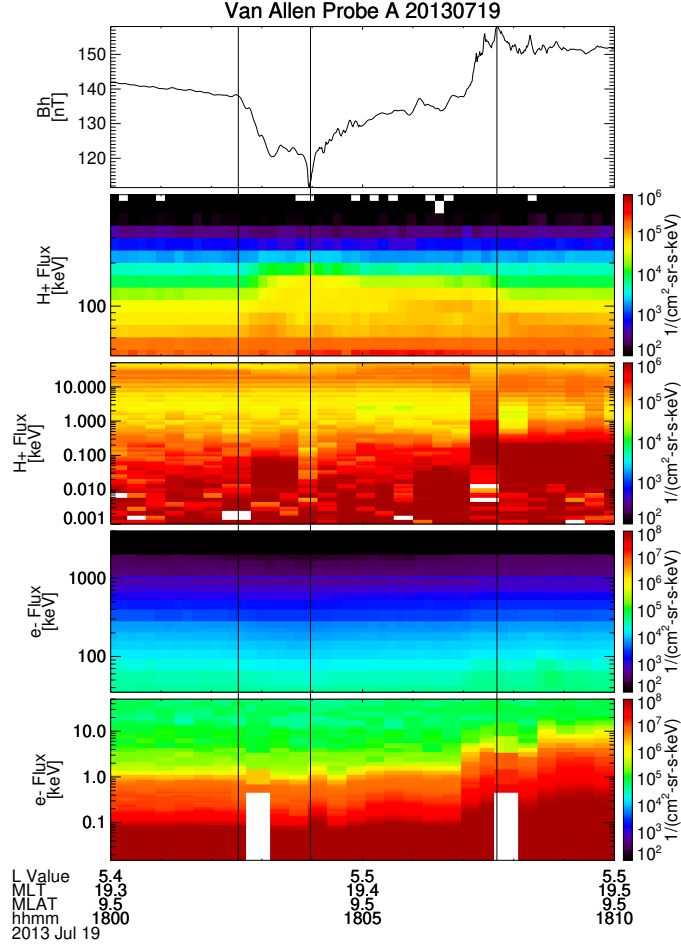


**Figure 2.** An overview plot for particle measurements during a dipolarization event starting at 18:03:58 UT on 19 July 2013. From top, the  $B_H$  component, high-energy proton fluxes from RBSPICE, low-energy proton fluxes from HOPE, high-energy electron fluxes from MagEIS, and low-energy electron fluxes from HOPE are plotted. Proton and electron fluxes from two instruments are plotted with a common color scale, respectively. Three vertical lines indicate the same times as in Figure 1.

173 activity started at 22:47 UT.  $AU$  and  $AL$  values reached 279 and  $-275$  nT, respectively,  
 174 at 22:52 UT. The  $Kp$  value was moderate with  $2^+$ . This event corresponded to the re-  
 175 recovery phase of a corotating interaction region (CIR)-driven geomagnetic storm. The min-  
 176 imum  $Dst$  value was  $-67$  nT at 8 UT on the previous day. After that  $Dst$  values grad-  
 177 ually recovered. At the time of the dipolarization, the value was  $-28$  nT. The IMF was  
 178 fluctuating due to the CIR encounter. The  $B_Z$  component was  $\sim -3$  to 0 nT around  
 179 the time of the event.

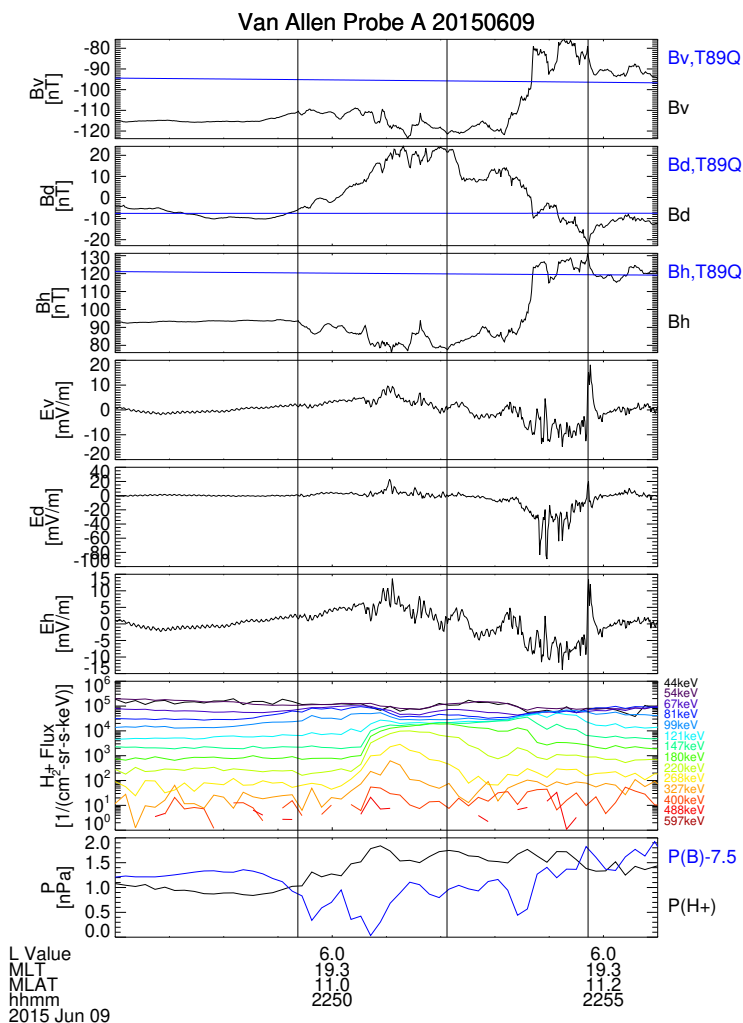


**Figure 3.** An overview plot for a dipolarization event starting at 22:52:07 UT on 9 June 2015, as observed by Van Allen Probe A. Magnetic fields, electric fields, and energetic protons are plotted in the same format as in Figure 1. Three vertical lines correspond to beginning of the dip, ending of the dip or beginning of the DF, and ending of the DF, respectively.

180 Figure 3 is an overview plot for magnetic and electric fields together with energetic  
 181 protons for this event. The northward magnetic field  $B_H$  started to decrease at 22:49:22  
 182 UT and reached minimum  $\sim$  22:52:07 UT, including some fluctuations. This interval  
 183 corresponds to the dip region. After that the  $B_H$  component increased to the maximum  
 184 at 22:54:43 UT, corresponding to the DF. The azimuthal magnetic field  $B_D$  increased  
 185 in the dip, while decreased in the DF. Since Probe A was located in the northern hemi-  
 186 sphere, the field line was displaced westward.

187 There were, again, electric field variations concurrent with magnetic field variations.  
 188 Outward and northward components were observed in the dip, while their signs were re-  
 189 versed in the DF. These correspond to westward and eastward motion of magnetic field  
 190 lines in the dip and DF, respectively. Westward electric field or outward motion was ob-  
 191 served in the dip, while larger, eastward electric field or inward motion was observed in  
 192 the DF.

193 Energetic proton pressure increased in the dip, while magnetic pressure was smaller  
 194 than neighboring values. In the DF, proton pressure decreased somewhat, while mag-  
 195 netic pressure increased more than that decrease.

196 It appears that the proton flux increased in two steps. The first increase started  
 197 gradually at  $\sim 22:48$  UT in the middle energy range of  $\sim 80 - 100$  keV. The second  
 198 increase was sharper and started at  $\sim 22:50$  UT near the minimum  $B_H$  at the energy  
 199 of  $\sim 120-400$  keV. These were similar to the observations by Gkioulidou et al. (2015)  
 200 and Motoba et al. (2021). Even though the second increase was sharp and at high en-  
 201 ergies, the pressure increase was larger at the first increase, due to the larger energy flux  
 202 of the middle energy component.

203 One possible reason for the two-step increase is that the energetic population within  
 204 a dipolarization structure consists of two parts. The one around the minimum  $B_H$  was  
 205 possibly related to the local dipolarization process, while another with the middle-energy  
 206 flux increase was due to the flux reflected at the DF (Zhou et al., 2011), as suggested  
 207 by Motoba et al. (2021). Reflected flux may be observed of the order of the ion gyro-  
 208 radius from the DF where such reflection occurs. Here we estimate typical values of equa-  
 209 torial gyroradius and gradient  $B$  drift speed as 310 km and 49 km/s, respectively, at the  
 210  $L$  value of 6.0 where probe A was located, assuming particle energy of 90 keV and the  
 211 dipole field. Probe A would traverse a structure with the gyroradius  $\sim 6$  s, which is much  
 212 shorter than the duration of the dip of the order of minutes. Here we assume that mo-  
 213 tion of the structure is of the order of the gradient  $B$  drift speed. There was not a sig-  
 214 nificant proton flux increase  $> \sim 100$  keV, at which the gyroradius is closer to the dip  
 215 length so that it is hard to explain the duration of the dip by local reflection.

216 Enhanced ions at  $\sim 80-100$  keV may not be locally reflected at the DF but prop-  
 217 agate from the magnetotail, where these ions were perhaps reflected. In order to exam-  
 218 ine this possibility, we refer to the observation reported by Zhou et al. (2011). Particle

219 fluxes of several tens of keV were enhanced in the magnetotail. The duration of the dip  
 220 could be explained by gyroradius of these ions divided by inward propagation velocity  
 221 there. If the magnetic moment is conserved during the transport process from the mag-  
 222 netotail to the Probe A's orbit, the perpendicular energy would be at most several keV,  
 223 while the parallel energy would be just below the original  $\sim 80\text{--}100$  keV, which is not  
 224 so realistic. Therefore, the pitch angle and possibly energy would change during the trans-  
 225 port process. Nonetheless, the ion flux in the dip observed by Probe A could be gener-  
 226 ated by the reflection process in the magnetotail. The longer duration of the dip in the  
 227 inner magnetosphere will be discussed again later.

228 The previous event on 19 July 2013 did not clearly show the two-step increase like  
 229 this event. Nonetheless, the peaks of the middle energy and high energy fluxes were slightly  
 230 offset in time. One possible reason for this is that the thickness of the dipolarization struc-  
 231 ture or its shape is different depending on the probe location relative to its center.

232 Figure 4 shows the particle measurements in detail. Particle signatures were over-  
 233 all similar to those on 19 July 2013. When energetic proton fluxes  $>\sim 60$  keV increased,  
 234 those around a few tens of keV decreased. Nonetheless, contribution to the pressure from  
 235 the former component was larger. Electron fluxes increased as the background magnetic  
 236 field increased.

237 For this event, Van Allen Probe B was located close to Probe A and observed the  
 238 dipolarization as well (Figure 5). The probe location was  $L = 5.9, 19.6$  MLT, and MLAT= $10.8$   
 239 deg. at 22:52:07 UT, when the dipolarization event started at Probe A. Probe B was lo-  
 240 cated inward with  $dL = -0.1$  and  $0.3$  h eastward in MLT. Although there were gaps  
 241 in electric field data, variations in magnetic fields, electric fields, and energetic protons  
 242 were similar to those observed by Probe A. Therefore, the spatial scale of the structure  
 243 was at least the separation distance between these two probes. There was a tendency  
 244 for Probe B to observe the dip and DF around several to several tens of s earlier than  
 245 Probe A, which could be explained by a westward propagation of the event.

## 246 4 Statistical Studies

247 In this section, we statistically analyze various properties of dipolarization events  
 248 with inductive, radial electric fields. Properties discussed include spatial occurrence, field  
 249 variations, pressure variations, and durations. We have collected a total of 22 events with

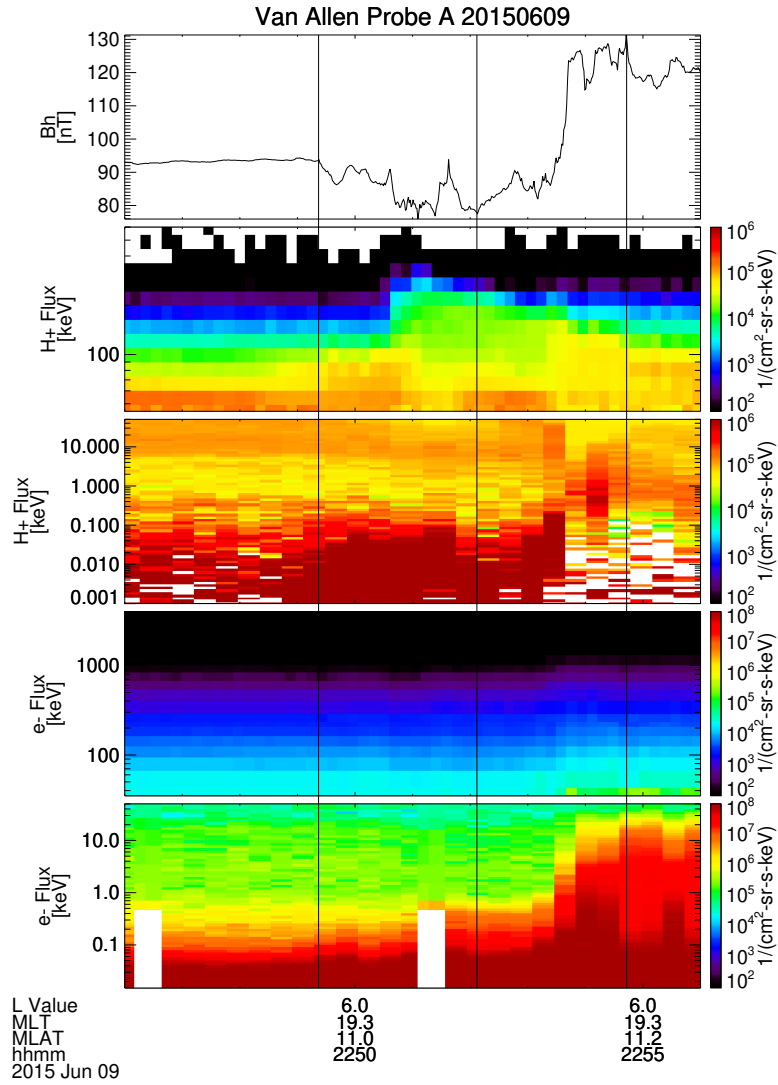


**Figure 4.** An overview plot for particle measurements for a dipolarization event starting at 22:52:07 UT on 9 June 2015. Horizontal magnetic fields  $B_H$  and proton and electron fluxes are plotted in the same format as in Figure 2. Three vertical lines indicate the same times as in Figure 3.

250 horizontal and vertical electric fields correlated with azimuthal magnetic fields with  $\sim$   
 251 90 deg. phase shift around the dipolarizations. These events are listed in the support-  
 252 ing information.

253 First, the spatial occurrence of these events are examined (left three panels of Fig-  
 254 ure 6). All events were observed between evening and premidnight MLTs. If energetic  
 255 protons are related to this type of dipolarization events, the MLT distribution could be

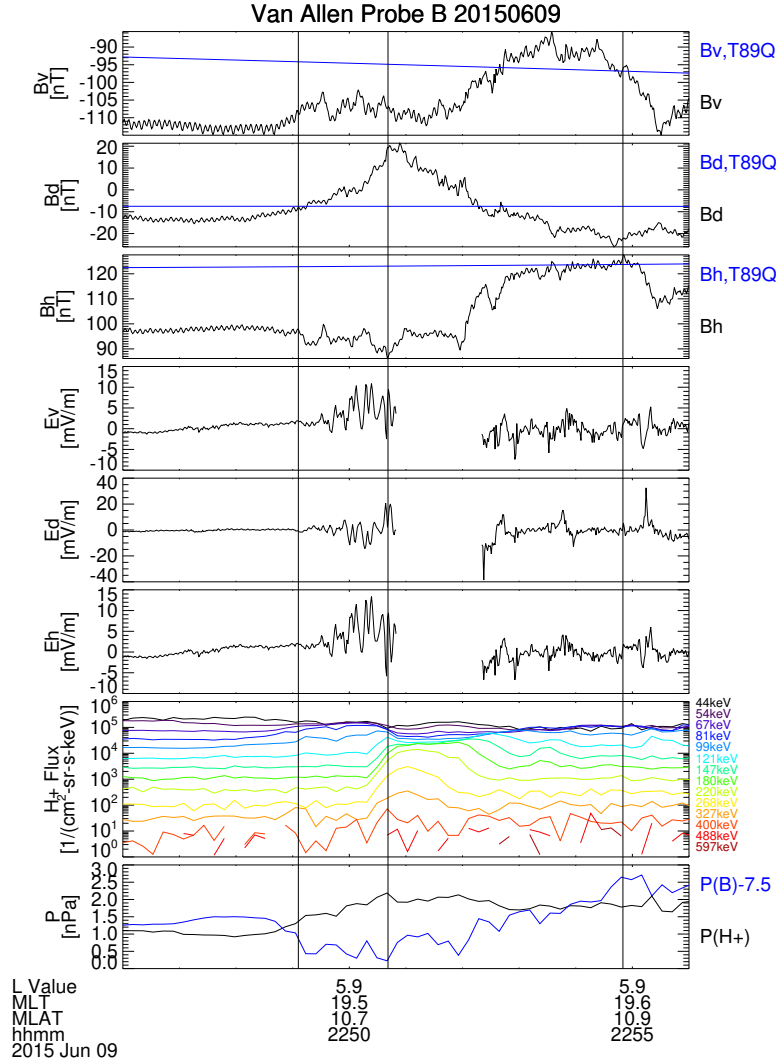


**Figure 5.** An overview plot for a dipolarization event starting at 22:50:41 UT on 9 June 2015, as observed by Van Allen Probe B. Magnetic fields, electric field, and energetic proton fluxes and pressure are plotted as in Figure 3. Three vertical lines indicate beginning of the dip, ending of the dip or beginning of the DF, and ending of the DF.

256 explained by these protons drifting westward in the inner magnetosphere. There is a slight  
 257 tendency for events to be observed at lower  $L$  shells in the evening MLT. There are no  
 258 significant features in the MLAT distribution. One possible reason is that Van Allen Probes'  
 259 orbits were relatively close to the magnetic equator with  $|\text{MLAT}| < 20$  deg.

260 The distribution of geomagnetic indices ( $AU$ ,  $AL$ ,  $Kp$ , and  $Dst$  indices) at the MLT  
 261 of each event is plotted in the right three panels. The events were observed during moderate  
 262 auroral electrojet ( $AE$ ) activities.  $AU$  values were as large as  $AL$  values in size so

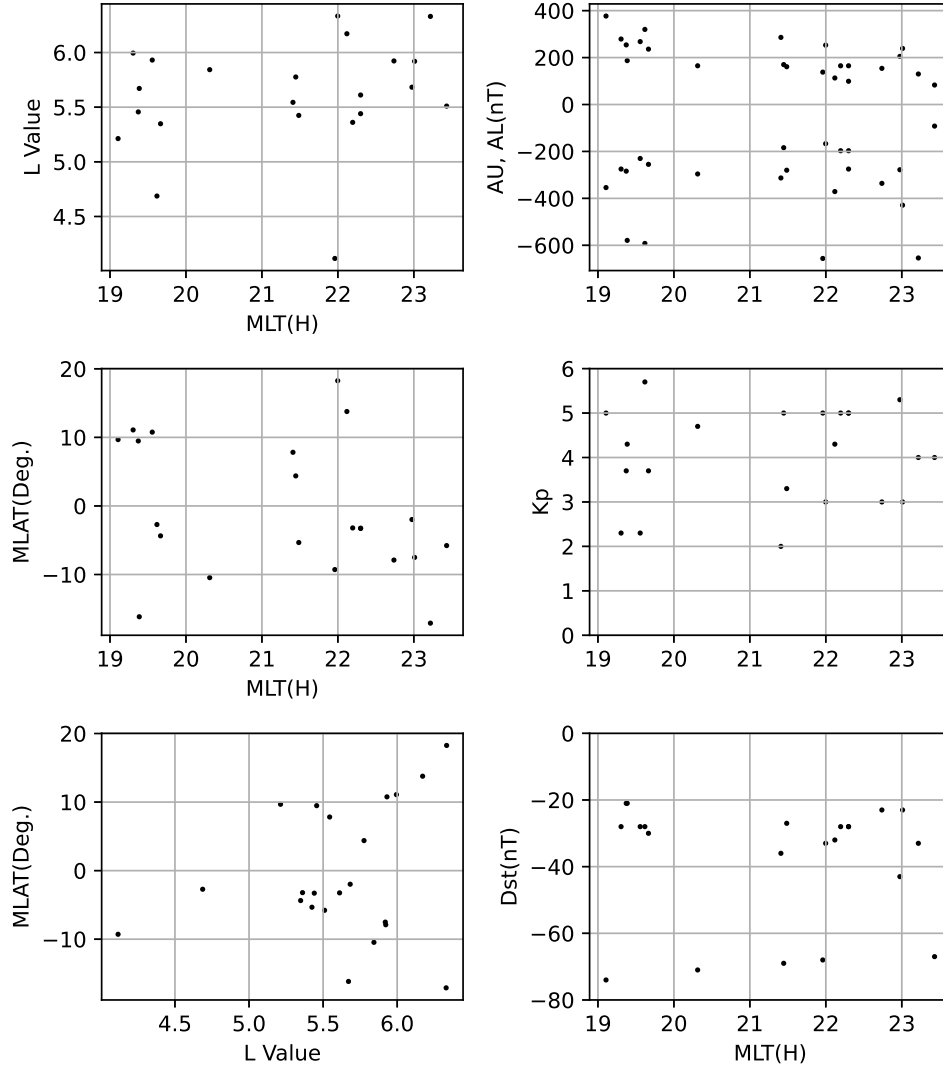


**Figure 6.** Left three panels show locations of dipolarization events organized by  $L$  value, MLT, or MLAT. Right three panels show geomagnetic activities ( $AU$ ,  $AL$ ,  $Kp$ , and  $Dst$  values) at MLT of each event.

263 that eastward electrojet was well developed. Since the eastward electrojet was expected  
 264 in the duskside magnetosphere, westward convection was also expected there, which is  
 265 a typical convection around that MLT during disturbed periods.  $Kp$  values were also  
 266 moderate.  $Dst$  values of some events were  $< -50$  nT, corresponding to geomagnetic storms,  
 267 while those of other events were  $> -50$  nT. Nonetheless, some minimum  $Dst$  values of  
 268 these other events were  $< -50$  nT around the time of the observation so that these events  
 269 also occurred during storms. In summary, about 70 % of the events (16/22 events) were

270 storm-time events. This, together with moderate  $AE$  and  $Kp$  values, could account for  
 271 the presence of dipolarization events at  $L$  shells inside geosynchronous orbit.

272 There is not much MLT dependence on geomagnetic activities. An exception could  
 273 be the  $AU$  index. Events observed in the eveningside tend to have larger  $AU$  values. This  
 274 could be due to well-developed eastward electrojet at that MLT. Perhaps, there was more  
 275 proton flux transport from the magnetotail.

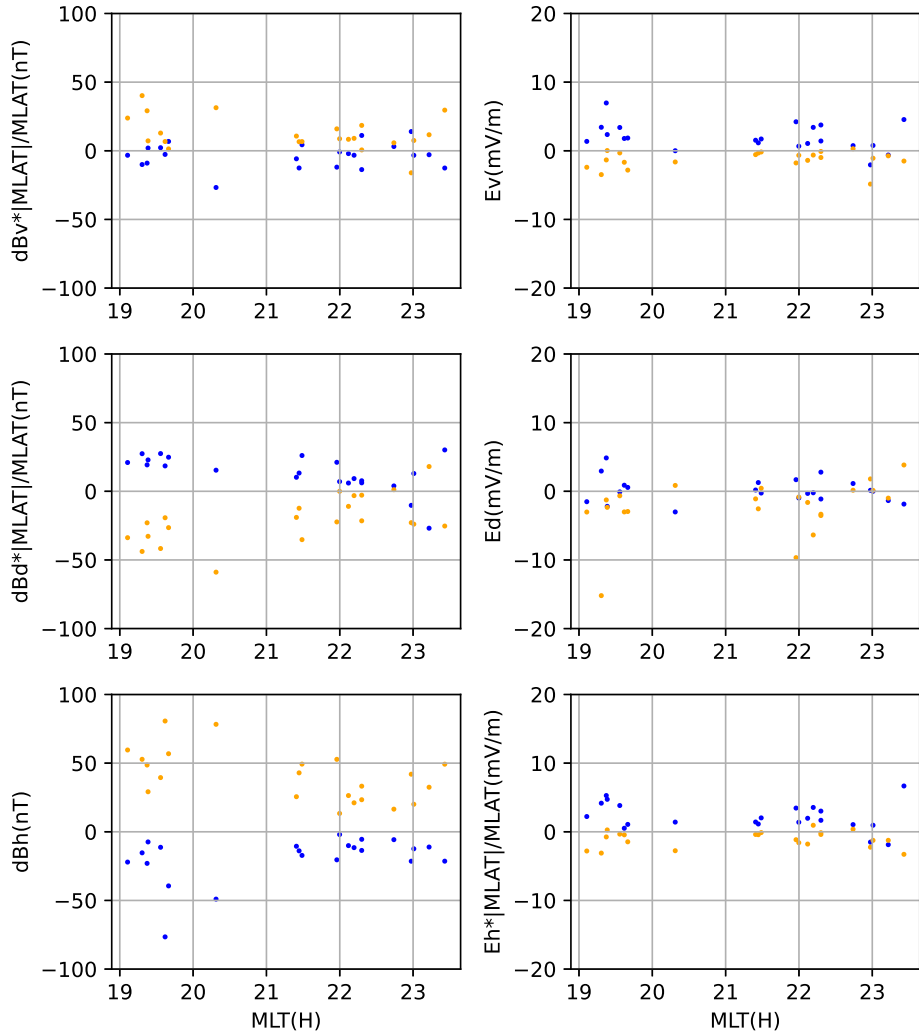


**Figure 7.** Distributions of each component of magnetic field variations and electric fields as a function of MLT. Blue and orange colors correspond to values calculated in the dip and DF, respectively. Signs of  $dB_V$ ,  $dB_D$ , and  $E_H$  components in the southern hemisphere are reversed, assuming symmetry of the structures between the hemispheres.

276 Next we show distributions of magnetic field variations and electric fields derived  
 277 for each event as a function of MLT (Figure 7). Magnetic field variations are calculated  
 278 as differences between final and initial values in the dip (blue) and the DF (orange), re-  
 279 spectively. Note that these colors are also used in later figures with the same meaning.  
 280 Quiet-time model values  $B_{T89Q}$  have already been subtracted so that the definition is  
 281  $dB \equiv (B - B_{T89Q})_{final} - (B - B_{T89Q})_{initial}$ . Average electric fields are calculated in  
 282 the dip and in the DF, respectively. These electric fields are contributed by variable com-  
 283 ponents because averages are calculated for shorter time scales than large-scale, back-  
 284 ground convection changes affected by the magnetosphere-ionosphere (M-I) coupling. Note  
 285 that there are partly gaps in electric field data in 7 of 22 events. Signs of  $dB_V$ ,  $dB_D$ , and  
 286  $E_H$  components are reversed for the events in the southern hemisphere because of sys-  
 287 tematic inter-hemispheric differences, if the structure is symmetric between the hemi-  
 288 spheres.

289 Signs of each field component were generally opposite between the dip and DF. Vari-  
 290 ations of magnetic fields were larger at an earlier MLT, which could be due to larger  $AU$   
 291 activities at that MLT, as mentioned before. Electric fields also had somewhat similar  
 292 MLT dependence as magnetic field variations. There was a tendency for  $E_V$  and  $E_H$  com-  
 293 ponents to be positive in the dip, while these were negative in the DF. This implies west-  
 294 ward field line motion in the dip, while field lines moved back eastward in the DF. The  
 295 medians of these electric fields are 2.2 mV/m in the dip and  $-1.6$  mV/m in the DF. If  
 296 converted to azimuthal  $E \times B$  drift velocity, they are  $-17$  km/s in the dip and 8 km/s  
 297 in the DF. The former velocity is not far from the gradient  $B$  drift velocity of energetic  
 298 protons so that these protons may be responsible for stretched field lines.

299 Signs of the  $dB_D$  component were generally the same as those of the  $E_V$  and  $E_H$   
 300 components, consistent with this idea of stretched field lines. Note that signs of the  $dB_D$   
 301 component are reversed in the southern hemisphere so that the magnetic field lines were  
 302 likely displaced most at the equator, while they were tied to the ionosphere. For exam-  
 303 ple, when field lines were moving westward at the equator, the electric field was outward.  
 304 Eastward magnetic field increased in the northern hemisphere, while westward magnetic  
 305 field did in the southern hemisphere. The shape of a field line was similar to that of fundamen-  
 306 tal-mode or odd harmonics of standing waves at least near the equator, where an anti-node  
 307 was located. The possibility of standing waves is discussed later. The latitudinal depen-  
 308 dence of the field line motion would be caused by energetic proton population trapped

309 around the equator. In addition, angular velocity of the gradient  $B$ /curvature drift of  
 310 particles at an energy is the largest at the equator (Lew, 1961).

311 The  $E_D$  value was less than the  $E_V$  or  $E_H$  value in the dip. The median is  $-0.043$   
 312 mV/m, while the median is  $-1.4$  mV/m in the DF.

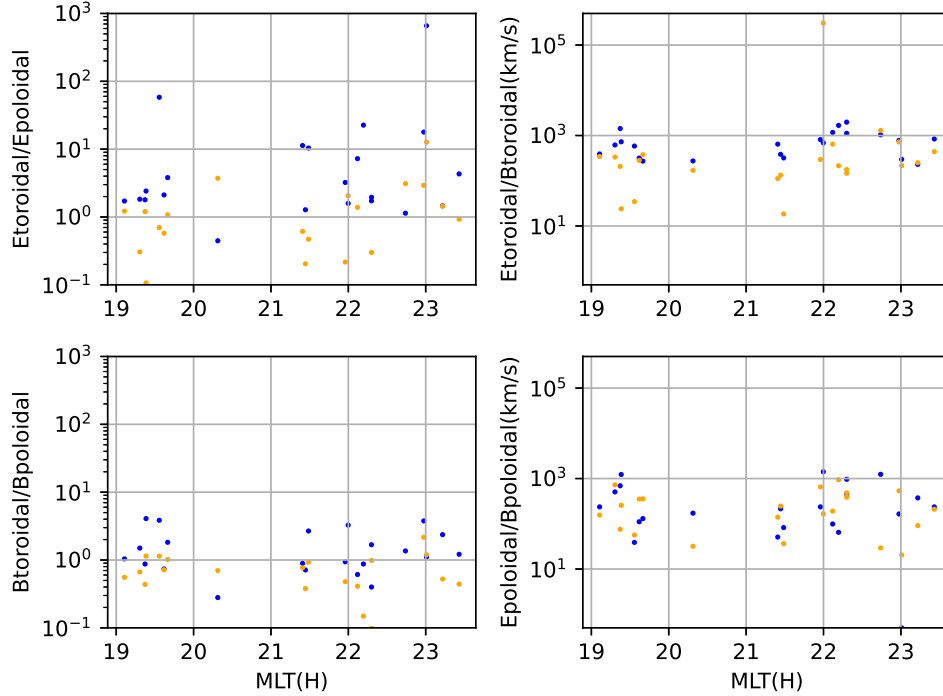


**Figure 8.** Left panels show ratios of toroidal components to poloidal components for magnetic fields (top) and electric fields (bottom). Right panels show  $E/B$  ratios of toroidal components (top) and poloidal components (bottom). Blue and orange colors correspond to the ratios at the dip and DF, respectively.

313 The ratios between toroidal and poloidal components are calculated for electric fields  
 314 and magnetic fields (left panels of Figure 8). Toroidal electric fields are approximated  
 315 to be in the plane perpendicular to the azimuthal direction and perpendicular to the back-  
 316 ground magnetic field component in that plane. Toroidal magnetic fields correspond to  
 317 the azimuthal component. Poloidal electric fields are also the azimuthal component, while  
 318 poloidal magnetic fields are defined in the same manner as the toroidal electric fields.  
 319 The ratios were often  $> 1$  for electric fields in the dip, implying the variations were mainly  
 320 toroidal. The ratios for magnetic fields were  $\sim 1$  because there were horizontal and ra-

321 dial magnetic field variations associated with the dip region itself in addition to the az-  
 322 imuthal ones. The ratios were smaller in the DF than in the dip. Electric fields in the  
 323 DF were more westward in addition to the inward component. Magnetic field variations  
 324 were more contributed by the horizontal and radial magnetic field increase.

325 Next, we discuss the  $E/B$  ratio calculated for toroidal and poloidal components  
 326 (right panels in Figure 8). Since the ratio of averaged electric fields  $E$  and differentiated  
 327 magnetic fields  $dB$  are not directly equivalent to the  $E/B$  ratio, we have multiplied a  
 328 factor  $\pi$  to  $E/dB$ . The above factor applies to an ideal case when the variation is sinu-  
 329 soidal and may be divided into two parts. In the first part, the factor 2 is introduced be-  
 330 cause magnetic field variations are calculated as differences between maximum and min-  
 331 imum values, while electric field variations are assumed to have only one sign. Note that  
 332 the phases between electric and magnetic fields are ideally shifted by 90 deg. In the sec-  
 333 ond part, the additional factor  $\pi/2$  is multiplied because electric fields assumed to be  
 334 sinusoidal are averaged, while magnetic field variations are not. However, the actual case  
 335 may be somewhat different so that the above factor is just only for reference.

336 There is not much MLT dependence of the  $E/B$  ratios. This is also the case for  
 337 the MLAT dependence (figure not shown). The latter implies that the property of the  
 338 structure to be inferred from this ratio, such as the spatial variation of standing waves,  
 339 if any, in the field-aligned direction, does not change much inside the Van Allen Probes'  
 340 orbits with  $|\text{MLAT}| < 20$  deg.

341 The toroidal  $E/B$  ratios in the dip were of the order of 1000 km/s or those of Alfvén  
 342 waves at where events were observed (e.g., McPherron, 2005) (Figure 8, top right). Since  
 343 there was a phase shift of  $\sim 90$  deg. between electric and magnetic fields, the waves would  
 344 not be propagating but standing. Nonetheless, the events were not likely to be solely the  
 345 fundamental mode or odd harmonics of the standing waves. If that were the case, the  
 346  $E/B$  ratio would be larger than that of propagating waves near the equator. The  $E/B$   
 347 ratio was also similar to that of the ionospheric structure (e.g., Gurnett et al., 1984). How-  
 348 ever, electric fields and magnetic fields are in phase in this case (e.g., Smiddy et al., 1980)  
 349 and we cannot explain the  $\sim 90$  deg. phase shift.

350 Another possibility is that an injected energetic proton structure drifted and in-  
 351 duced field line motion. This inference is applicable to stretched magnetic field lines dis-  
 352 cussed above. In this case, the  $E/B$  ratio is  $VB/dB$ . Even though the motional veloc-

353 ity  $V$  of field lines was smaller than the phase velocity of Alfvén waves, the magnetic field  
 354 variation  $dB$  was also smaller than the background magnetic field  $B$ . A large range of  
 355 values are possible for the  $E/B$  ratio, taking into account the dependence of this struc-  
 356 ture and its field line motion on latitudes. The phase shift may be  $\sim 90$  deg. based on  
 357 the spatial and temporal variation of this structure. Standing Alfvén waves may over-  
 358 lap. The  $E/B$  ratio contributed by the drifting structure and the standing waves would  
 359 not necessarily be larger than the Alfvén velocity.

360 In the DF, the toroidal  $E/B$  ratio was smaller than that in the dip. The electric  
 361 field decrease as well as the magnetic field increase contributed to the smaller ratio. Nonethe-  
 362 less, the drifting proton structure as well as standing waves possibly contributed to the  
 363 observed  $E/B$  ratio, similar to the variations in the dip. On top of these structures and  
 364 waves, there could be higher harmonics of standing waves in the DF because the field  
 365 variations were irregular, particularly for electric fields as shown in the case study. The  
 366  $E/B$  ratio at higher frequencies up to 0.5 Hz is calculated and there was a tendency for  
 367 this ratio to be larger than the one at lower frequencies derived above and to be closer  
 368 to the typical Alfvén velocity (figure not shown). The larger  $E/B$  ratio is possibly be-  
 369 cause there was a larger contribution from higher harmonics to the field variations than  
 370 the drifting energetic proton structures. Note that the  $E/B$  ratio is expected to be closer  
 371 to the Alfvén velocity, if more harmonics overlap.

372 Standing waves during dipolarization events or substorms have previously been re-  
 373 ported (Takahashi et al., 1988). Since the duration of the dip and DF was of the order  
 374 of minutes or the Alfvén transit time between the magnetic equator and the ionosphere,  
 375 there could be standing waves. Standing waves with kinetic effects during dipolarization  
 376 events have been previously reported by Van Allen Probes (Chaston et al., 2014) and  
 377 MMS (Matsui et al., 2016). Field variations are irregular in this case because there are  
 378 multiple frequency or wavelength components. As already mentioned, electric field vari-  
 379 ations examined were irregular in the DF. In addition, parallel Poynting flux at higher  
 380 frequencies up to 0.5 Hz is calculated and its standard deviations are larger than or close  
 381 to average values. The direction of the Poynting flux along the magnetic field was vari-  
 382 able, again implying that the field variation was irregular. Note also that the events stud-  
 383 ied here were observed by Van Allen Probes where the background magnetic field is dipole-  
 384 like, in which Samson et al. (1992) inferred that there are standing waves with kinetic  
 385 effects.

386 Concerning the poloidal  $E/B$  ratio (Figure 8, bottom right), the values were smaller  
 387 than those of the toroidal ratio in the dip possibly because the electric field variation was  
 388 mainly toroidal. In the DF, the poloidal ratio was similar to the toroidal ratio, imply-  
 389 ing the variation was more isotropic.

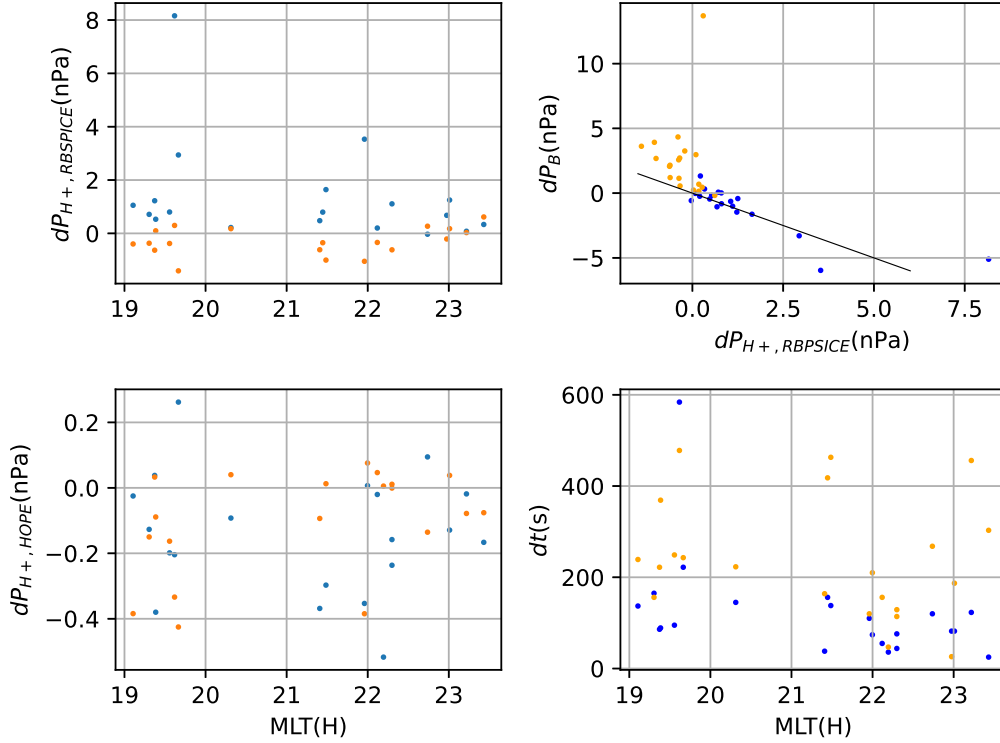


**Figure 9.** Left two panels show proton pressure variations either in the dip or DF, as measured by RBSVICE (top) and HOPE (bottom) and organized by MLT. The top right panel is a scatter plot between proton pressure variations measured by RBSVICE and magnetic pressure variations. The black line indicates where proton pressure variations are balanced by magnetic pressure variations with an opposite sign. The bottom right panel shows durations of the dip and DF as a function of MLT. The blue and orange colors in each panel correspond to the values in the dip and DF, respectively.

390 Proton pressure variations are derived in the RBSVICE energy range (40-800 keV)  
 391 and the HOPE energy range (30 eV-50 keV) (Left two panels in Figure 9). Variations  
 392 are calculated as differences between final and initial values in either the dip or DF. When  
 393 there are no RBSVICE moments (3/22 events) or HOPE moments (2/22 events), we do  
 394 not show results from each instrument. Proton pressure generally increased in the dip

395 in the RBSPICE energy range and decreased in the DF. Proton pressure decreased both  
 396 in the dip and DF in the HOPE energy range. Proton pressure variations in the RBSPICE  
 397 energy range were larger than those in the HOPE energy range. Proton pressure increases  
 398 in the RBSPICE energy range were often balanced by magnetic pressure decreases in the  
 399 dip (top right panel) so that total pressure did not change much. If the magnetic field  
 400 variations gradually changed along magnetic field lines, the structure would be close to  
 401 static. Proton pressure decreases were smaller than magnetic pressure increases in the  
 402 DF so that the field variations were probably more variable in time than those in the dip.  
 403 These proton pressure variations may contribute to a source term to generate Alfvén waves  
 404 (Kivelson & Southwood, 1991). The idea of drifting particle structures, and in addition  
 405 standing waves, inferred from the electric and magnetic field statistics, is consistent with  
 406 this analysis.

407 Note that not all of the dipolarization events with inductive, radial electric fields  
 408 are explained by the above idea of drifting energetic proton structure. For example, there  
 409 were two events in the dip with  $E_V < 0$  close to the midnight. Since proton pressure  
 410 increased, these events may not be explained as the above. We have also checked whether  
 411 electron pressure increased, supporting  $E_V < 0$  because of the opposite drift direction  
 412 to protons, but do not always find that signature. Some other explanation such as the  
 413 radial variation of the structure, including the structure moving inward, needs to be in-  
 414 troduced.

415 The bottom right panel of Figure 9 shows durations of the dip and DF as a func-  
 416 tion of MLT. These durations were generally longer in the earlier MLTs. Since there was  
 417 a tendency for the background magnetic fields to be larger in the eveningside because  
 418 of inner  $L$  shells of event locations, the observed durations could be explained by this  
 419 effect, if the convection electric field did not change much with MLT. Another possibil-  
 420 ity is the difference in drift velocity between the middle-energy ions and the magnetic  
 421 flux associated with the dipolarization. The former is thought to be moving with the gra-  
 422 dient  $B$ /curvature drift velocity in addition to the  $E \times B$  drift velocity, while the lat-  
 423 ter is moving with the  $E \times B$  drift velocity. Once the event arrives at the nightside in-  
 424 ner magnetosphere from the magnetotail, the time difference between both structures  
 425 increases as the MLT shifts toward the eveningside.

426 The longer durations of the dip in the eveningside could be consistent with Nagai  
 427 (1982), in which the beginning of the  $B_H$  increase was more delayed from the substorm  
 428 onset when a geosynchronous spacecraft was located further away from midnight. Note  
 429 that the substorm onset in that study was identified by low- and middle-latitude ground  
 430 magnetometers and was approximately simultaneous to the beginning of the azimuthal  
 431 magnetic field variation. The coincidence of the beginning of the azimuthal magnetic field  
 432 variation and that of the dip was observed in our case study.

433 If the longer duration of the dip in the eveningside would be caused by the differ-  
 434 ent drift speed mentioned above, this may complement the explanation of the dip as be-  
 435 ing due to reflected ions at the DF in the magnetotail. This is because the reflection pro-  
 436 cess would contribute to an offset to the dip durations, while their MLT dependence is  
 437 due to the gradient  $B$ /curvature drift of middle-energy ions. Durations of the dip had  
 438 offset values in the premidnight MLT in the figure.

439 Lastly, the MVA of magnetic fields (Sonnerup & Scheible, 1998) is performed to  
 440 investigate characteristics of variable fields. An analysis period for an event includes the  
 441 dip and DF. The  $L$  direction is defined to be positive in the northward direction, while  
 442 the  $N$  direction is positive in the sunward direction. Eigenvalue ratios  $\lambda_1/\lambda_2$  are larger  
 443 in the evening MLT (top left panel of Figure 10), where  $\lambda_1$  and  $\lambda_2$  are maximum and  
 444 intermediate eigenvalues, respectively. This is related to larger fluctuations in  $B_H$  and  
 445  $B_D$  components around this MLT. These ratios decrease in the premidnight MLT, while  
 446 the ratios  $\lambda_2/\lambda_3$  tend to increase. Here  $\lambda_3$  is a minimum eigenvalue. Fluctuations were  
 447 more two-dimensional in the plane including  $H$  and  $D$  directions. Angles of  $L$  and  $N$   
 448 directions from the background magnetic fields are calculated when  $\lambda_1/\lambda_2 > 3$  and  $\lambda_2/\lambda_3 >$   
 449  $3$ , respectively (bottom left panel).  $L$  directions tend to be parallel to the background  
 450 fields near the equator at  $|\text{MLAT}| < \sim 5$  deg. and perpendicular outside the equator.  
 451  $N$  directions are perpendicular to the background fields near the equator and parallel  
 452 outside the equator. Therefore, dipolarizations were more compressional near the equa-  
 453 tor, while magnetic variations were more transverse off the equator possibly because of  
 454 larger background magnetic fields along a magnetic field line.

455 Elevation and azimuth angles of  $L$  directions are plotted in  $VDH$  coordinates when  
 456  $\lambda_1/\lambda_2 > 3$  and  $L$  directions are quasi-perpendicular  $> 45$  deg. to background magnetic  
 457 fields (top right panel). Azimuth angles are often  $\sim 90$  deg., implying that maximum

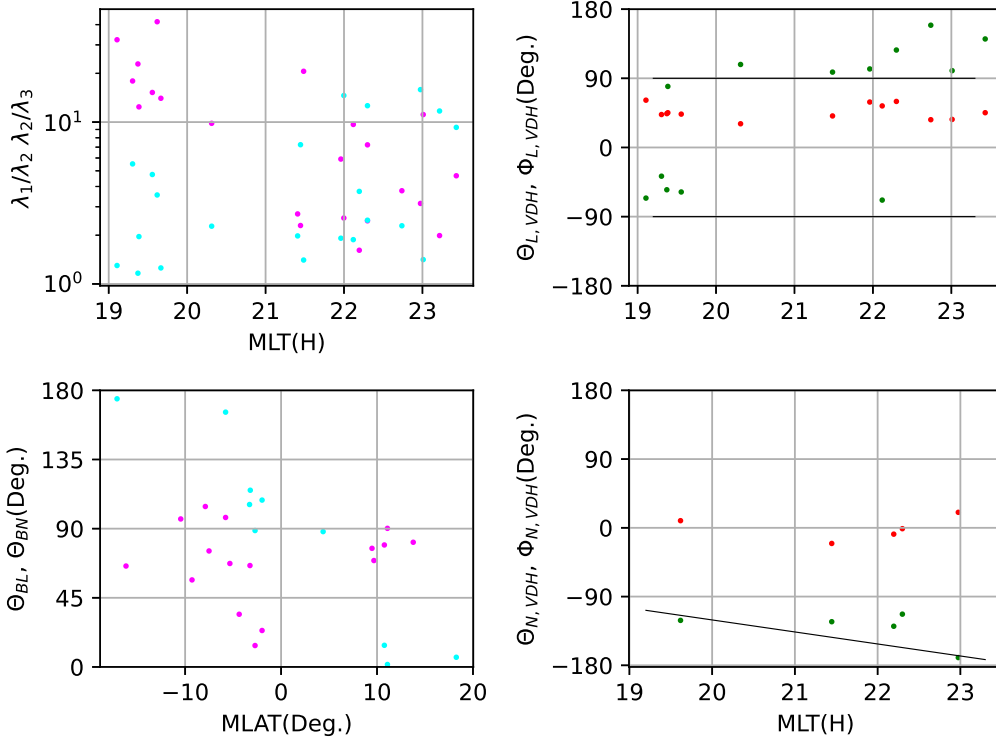


**Figure 10.** Results from the minimum variance analysis (MVA) for our dipolarization events. The top left panel shows eigenvalue ratios  $\lambda_1/\lambda_2$  and  $\lambda_2/\lambda_3$  as a function of MLT in magenta and cyan colors, respectively. The bottom left panel shows angles of  $L$  and  $N$  directions from background magnetic fields as a function of MLAT in magenta and cyan colors, when  $\lambda_1/\lambda_2 > 3$  and  $\lambda_2/\lambda_3 > 3$ , respectively. The right two panels show  $L$  and  $N$  directions in  $VDH$  coordinates as a function of MLT, when the above condition for eigenvalue ratios is satisfied and directions are  $> 45$  deg. from background magnetic fields. Elevation and azimuth angles are plotted in red and green colors, respectively. Black lines indicate where  $L$  directions are azimuthal (top right panel) and  $N$  directions are sunward (bottom right panel).

458 variations include azimuthal variations related to field-line stretching off the equator. Sim-  
 459 ilarly, elevation and azimuth angles of  $N$  directions are plotted when  $\lambda_2/\lambda_3 > 3$  and  
 460  $N$  directions are quasi-perpendicular (bottom right panel). Azimuth angles tend to align  
 461 to the  $X$  or  $D$  direction. It is hard to distinguish between these because number of data  
 462 points is not large. This implies the structure propagated in the sunward or westward  
 463 direction.

## 5 Summary and Conclusions

Two case studies of dipolarization events with inductive, radial electric fields were presented. In addition, a total of 22 dipolarization events have been collected and statistically analyzed. These events were observed between evening and premidnight MLTs and were accompanied by energetic proton increases. When there were no RBSPICE data, MAGEIS instruments, also measuring ions, observed such increases  $> 60$  or  $> 160$  keV. The events occurred during moderate geomagnetic activities. About 70 % of them corresponded to geomagnetic storms. In general, signs of each component of magnetic and electric field variations were opposite between the dip and DF. Field line motion in the dip was similar to the gradient  $B$ /curvature drift velocities of energetic protons. Plasma pressure increased in the dip and decreased in the DF. Durations of the DF were longer in the earlier MLT. According to the MVA, variations were more compressional near the equator.

Below is one possible explanation for the overall characteristics of magnetic and electric field variations and energetic protons in the dip. Since these magnetic field variations appeared with energetic proton injections and the field line motion was similar to the gradient  $B$ /curvature drift velocities of these protons, the field line would be stretched by these protons. One possibility is that these energetic protons were reflected at the DF in the magnetotail and subsequently transported to the inner magnetosphere. Referring to the azimuthal magnetic field variation which was opposite between hemispheres, the magnetic field line was most stretched westward around the equator. This is because there were trapped energetic populations with their largest drift around the equator. Fundamental mode or odd harmonics of standing waves could be generated.

In the DF, field variations were more irregular. It is inferred that there were standing waves with higher harmonics. Convection turned to eastward in the DF possibly because field lines may not be stretched further. The field lines previously in the dip may collide with those in the westward location so that magnetic and electric field variations may become turbulent with kinetic effects. The horizontal magnetic field started to increase with energetic protons for the event on 9 June 2015. The energy was larger than that of middle-energy protons in the dip. The higher-energy protons near the minimum  $B_H$  would be accelerated by local processes, such as the interaction of populations trapped around the DF with electric field induced by the DF motion (Ukhorskiy et al., 2017).

Possible future study may be performed with MMS data set (Burch et al., 2016), which is now growing. Multi-spacecraft data analyses such as the timing analysis and the curlometer technique could work. Sub-ion scale structures may also be analyzed. Although low-energy populations are often not measured, these do not contribute much to the pressure in the inner magnetosphere so that analyses with high-energy populations would be sufficient.

## 6 Open Research

Van Allen Probes data are publicly available at <https://emfisis.physics.uiowa.edu/>, <http://space.umn.edu/missions/rbspew-home-university-of-minnesota/>, <http://rbspice.ftecs.com/>, and <https://cdaweb.gsfc.nasa.gov/>. *AE* and *Dst* indices are available at <https://wdc.kugi.kyoto-u.ac.jp/> (Nose et al., 2015a, 2015b). *Kp* index may be downloaded at <https://www.gfz-potsdam.de/en/kp-index/> (Matzka, Bronkalla, et al., 2021). OMNI data are available at <https://omniweb.gsfc.nasa.gov/> (Papitashvili & King, 2020).

The data analysis software to generate figures in this study is available on Zenodo (Matsui & Farrugia, 2022).

## Acknowledgments

This work was supported by NASA’s Van Allen Probes Contract NAS5-01072 and NASA Grant 80NSSC22K0526.

## References

- Baker, D. N., Belian, R. D., Higbie, P. R., & Hones, E. W., Jr. (1979). High-energy magnetospheric protons and their dependence on geomagnetic and interplanetary conditions. *Journal of Geophysical Research*, *84*, 7138–7154. doi: <https://doi.org/10.1029/JA084iA12p07138>
- Birn, J., Thomsen, M. F., Borovsky, J. E., Reeves, G. D., McComas, D. J., & Belian, R. D. (1997). Characteristic plasma properties during dispersionless substorm injections at geosynchronous orbit. *Journal of Geophysical Research*, *102*, 2309–2324. doi: <https://doi.org/10.1029/96JA02870>
- Blake, J. B., Carranza, P. A., Claudepierre, S. G., Clemmons, J. H., Crain, W. R., Jr., Dotan, Y., et al. (2013). The Magnetic Electron Ion Spectrometer

- 525 (MagEIS) instruments aboard the Radiation Belt Storm Probes (RBSP) space-  
526 craft. *Space Science Reviews*, 179, 383–421. doi: [https://doi.org/10.1007/  
527 s11214-013-9991-8](https://doi.org/10.1007/s11214-013-9991-8)
- 528 Burch, J. L., Moore, T. E., Torbert, R. B., & Giles, B. L. (2016). Magnetospheric  
529 Multiscale overview and science objectives. *Space Science Reviews*, 199, 5–21.  
530 doi: <https://doi.org/10.1007/s11214-015-0164-9>
- 531 Chaston, C. C., Bonnell, J. W., Wygant, J. R., Mozer, F., Bale, S. D., Kersten, K.,  
532 et al. (2014). Observations of kinetic scale field line resonances. *Geophysical  
533 Research Letters*, 41, 209–215. doi: <https://doi.org/10.1002/2013GL058507>
- 534 Cummings, W. D., Barfield, J. N., & Coleman, P. J., Jr. (1968). Magnetospheric  
535 substorms observed at the synchronous orbit. *Journal of Geophysical Research*,  
536 73, 6687–6698. doi: <https://doi.org/10.1029/JA073i021p06687>
- 537 Ergun, R. E., Goodrich, K. A., Stawarz, J. E., Andersson, L., & Angelopoulos,  
538 V. (2015). Large-amplitude electric fields associated with bursty bulk flow  
539 breaking in the Earth’s plasma sheet. *Journal of Geophysical Research: Space  
540 Physics*, 120, 1832–1844. doi: <https://doi.org/10.1002/2014JA020165>
- 541 Funsten, H. O., Skoug, R. M., Guthrie, A. A., MacDonald, E. A., Baldonado, J. R.,  
542 Harper, R. W., et al. (2013). Helium, Oxygen, Proton, and Electron (HOPE)  
543 mass spectrometer for the Radiation Belt Storm Probes mission. *Space Science  
544 Reviews*, 179, 423–484. doi: <https://doi.org/10.1007/s11214-013-9968-7>
- 545 Gkioulidou, M., Ohtani, S., Mitchell, D. G., Ukhorskiy, A. Y., Reeves, G. D.,  
546 Turner, D. L., et al. (2015). Spatial structure and temporal evolution of  
547 energetic particle injections in the inner magnetosphere during the 14 July  
548 2013 substorm event. *Journal of Geophysical Research: Space Physics*, 120,  
549 1924–1938. doi: <https://doi.org/10.1002/2014JA020872>
- 550 Gurnett, D. A., Huff, R. L., Menietti, J. D., Burch, J. L., Winningham, J. D., &  
551 Shawhan, S. D. (1984). Correlated low-frequency electric and magnetic noise  
552 along the auroral field lines. *Journal of Geophysical Research*, 89, 8971–8985.  
553 doi: <https://doi.org/10.1029/JA089iA10p08971>
- 554 Kepko, L., McPherron, R. L., Amm, O., Apatenkov, S., Baumjohann, W., Birn, J.,  
555 et al. (2015). Substorm current wedge revisited. *Space Science Reviews*, 190,  
556 1–46. doi: <https://doi.org/10.1007/s11214-014-0124-9>
- 557 King, J. H., & Papitashvili, N. E. (2005). Solar wind spatial scales in and com-

- 558        comparisons of hourly Wind and ACE plasma and magnetic field data.        *Jour-*  
559        *nal of Geophysical Research*, *110*, A02104.        doi: [https://doi.org/10.1029/](https://doi.org/10.1029/2004JA010649)  
560        2004JA010649
- 561        Kivelson, M. G., & Southwood, D. J.        (1991).        Ionospheric traveling vortex genera-  
562        tion by solar wind buffeting of the magnetosphere.        *Journal of Geophysical Re-*  
563        *search*, *96*, 1661–1667. doi: 10.1029/90JA01805
- 564        Kletzing, C. A., Kurth, W. S., Acuna, M., MacDowall, R. J., Torbert, R. B.,  
565        Averkamp, T., et al.        (2013).        The Electric and Magnetic Field Instrument  
566        Suite and Integrated Science (EMFISIS) on RBSP.        *Space Science Reviews*,  
567        *179*, 127–181. doi: <https://doi.org/10.1007/s11214-013-9993-6>
- 568        Lew, J. S.        (1961).        Drift rate in a dipole field.        *Journal of Geophysical Research*, *66*,  
569        2681–2685. doi: <https://doi.org/10.1029/JZ066i009p02681>
- 570        Liu, J., Angelopoulos, V., Zhang, X.-J., Turner, D. L., Gabrielse, C., Runov, A.,  
571        et al.        (2016).        Dipolarizing flux bundles in the cis-geosynchronous magne-  
572        tosphere: Relationship between electric fields and energetic particle injec-  
573        tions.        *Journal of Geophysical Research: Space Physics*, *121*, 1362–1376. doi:  
574        <https://doi.org/10.1002/2015JA021691>
- 575        Matsui, H., Erickson, P. J., Foster, J. C., Torbert, R. B., Argall, M. R., Ander-  
576        son, B. J., et al.        (2016).        Dipolarization in the inner magnetosphere during  
577        a geomagnetic storm on 7 October 2015.        *Geophysical Research Letters*, *43*,  
578        9397–9405. doi: <https://doi.org/10.1002/2016GL070677>
- 579        Matsui, H., & Farrugia, C. J.        (2022).        *Data Analysis Software for Dipolarization*  
580        *Events With Inductive, Radial Electric Fields Observed by Van Allen Probes.*  
581        *V. 1.0. [Software].* Zenodo. doi: <https://doi.org/10.5281/zenodo.7261397>
- 582        Matzka, J., Bronkalla, O., Tornow, K., Elger, K., & Stolle, C.        (2021).        *Geomagnetic*  
583        *Kp index. V. 1.0. [Dataset].* GFZ Data Services. doi: [https://doi.org/10.5880/](https://doi.org/10.5880/Kp.0001)  
584        Kp.0001
- 585        Matzka, J., Stolle, C., Yamazaki, Y., Bronkalla, O., & Morschhauser, A.        (2021).  
586        The geomagnetic *Kp* index and derived indices of geomagnetic activity.        *Space*  
587        *Weather*, *19*, e2020SW002641. doi: <https://doi.org/10.1029/2020SW002641>
- 588        Mauk, B. H., Fox, N. J., Kanekal, S. G., Kessel, R. L., Sibeck, D. G., & Ukhorskiy,  
589        A.        (2013).        Science objectives and rationale for the Radiation Belt Storm  
590        Probes mission.        *Space Science Reviews*, *179*, 3–27.        doi: <https://doi.org/>

- 591 10.1007/s11214-012-9908-y
- 592 McPherron, R. L. (2005). Magnetic pulsations: Their sources and relation to so-  
 593 lar wind and geomagnetic activity. *Surveys in Geophysics*, *26*, 545–592. doi:  
 594 <https://doi.org/10.1007/s10712-005-1758-7>
- 595 McPherron, R. L., Russell, C. T., & Aubry, M. P. (1973). Satellite studies of  
 596 magnetospheric substorms on August 15, 1968 9. Phenomenological model  
 597 for substorms. *Journal of Geophysical Research*, *78*, 3131–3149. doi:  
 598 <https://doi.org/10.1029/JA078i016p03131>
- 599 Mitchell, D. G., Lanzerotti, L. J., Kim, C. K., Stokes, M., Ho, G., Cooper, S., et  
 600 al. (2013). Radiation Belt Storm Probes Ion Composition Experiment (RB-  
 601 SPICE). *Space Science Reviews*, *179*, 263–308. doi: <https://doi.org/10.1007/s11214-013-9965-x>
- 602
- 603 Motoba, T., Ohtani, S., Gkioulidou, M., Ukhorskiy, A. Y., Lanzerotti, L. J., &  
 604 Claudepierre, S. G. (2021). Superposed epoch analysis of dispersionless particle  
 605 injections inside geosynchronous orbit. *Journal of Geophysical Research: Space*  
 606 *Physics*, *126*, e2021JA029546. doi: <https://doi.org/10.1029/2021JA029546>
- 607 Nagai, T. (1982). Observed magnetic substorm signatures at synchronous altitude.  
 608 *Journal of Geophysical Research*, *87*, 4405–4417. doi: <https://doi.org/10.1029/JA087iA06p04405>
- 609
- 610 Nakamura, R., Baumjohann, W., Klecker, B., Bogdanova, Y., Balogh, A., Rème,  
 611 H., et al. (2002). Motion of the dipolarization front during a flow burst  
 612 event observed by Cluster. *Geophysical Research Letters*, *29*, 1942. doi:  
 613 <https://doi.org/10.1029/2002GL015763>
- 614 Nose, M., Iyemori, T., Sugiura, M., & Kamei, T. (2015a). *Geomagnetic AE index*.  
 615 World Data Center for Geomagnetism, Kyoto. doi: <https://doi.org/10.17593/15031-54800>
- 616
- 617 Nose, M., Iyemori, T., Sugiura, M., & Kamei, T. (2015b). *Geomagnetic Dst index*.  
 618 World Data Center for Geomagnetism, Kyoto. doi: <https://doi.org/10.17593/14515-74000>
- 619
- 620 Papitashvili, N. E., & King, J. H. (2020). *OMNI 1-min Data [Dataset]*. NASA Space  
 621 Physics Data Facility. doi: <https://doi.org/10.48322/45bb-8792>
- 622 Runov, A., Angelopoulos, V., Zhou, X.-Z., Zhang, X.-J., Li, S., Plaschke, F., & Bon-  
 623 nell, J. (2011). A THEMIS multicase study of dipolarization fronts in the

- 624 magnetotail plasma sheet. *Journal of Geophysical Research*, *116*, A05216. doi:  
625 <https://doi.org/10.1029/2010JA016316>
- 626 Samson, J. C., Wallis, D. D., Hughes, T. J., Creutzberg, F., Ruohoniemi, J. M., &  
627 Greenwald, R. A. (1992). Substorm intensifications and field line resonances in  
628 the nightside magnetosphere. *Journal of Geophysical Research*, *97*, 8495–8518.  
629 doi: <https://doi.org/10.1029/91JA03156>
- 630 Schmid, D., Volwerk, M., Plaschke, F., Nakamura, R., Baumjohann, W., Wang,  
631 G. Q., et al. (2019). A statistical study on the properties of dips ahead of  
632 dipolarization fronts observed by MMS. *Journal of Geophysical Research:*  
633 *Space Physics*, *124*, 139–150. doi: <https://doi.org/10.1029/2018JA026062>
- 634 Sergeev, V. A., Angelopoulos, V., & Nakamura, R. (2012). Recent advances in  
635 understanding substorm dynamics. *Geophysical Research Letters*, *39*, L05101.  
636 doi: <https://doi.org/10.1029/2012GL050859>
- 637 Smiddy, M., Burke, W. J., Kelley, M. C., Saflekos, N. A., Gussenhoven, M. S.,  
638 Hardy, D. A., & Rich, F. J. (1980). Effects of high-latitude conductivity on  
639 observed convection electric fields and Birkeland currents. *Journal of Geophys-*  
640 *ical Research*, *85*, 6811–6818. doi: <https://doi.org/10.1029/JA085iA12p06811>
- 641 Sonnerup, B. U. O., & Scheible, M. (1998). Minimum and maximum variance  
642 analysis. In G. Paschmann & P. W. Daly (Eds.), *Analysis methods for multi-*  
643 *spacecraft data* (pp. 185–220). Noordwijk, The Netherlands: ESA Publications  
644 Division.
- 645 Takahashi, K., Kokubun, S., Sakurai, T., McEntire, R. W., Potemra, T. A., &  
646 Lopez, R. E. (1988). AMPTE/CCE observations of substorm-associated  
647 standing Alfvén waves in the midnight sector. *Geophysical Research Letters*,  
648 *15*, 1287–1290. doi: <https://doi.org/10.1029/GL015i011p01287>
- 649 Tian, S., Colpitts, C. A., Wygant, J. R., Cattell, C. A., Ferradas, C. P., Igl, A. B.,  
650 et al. (2021). Evidence of Alfvénic Poynting flux as the primary driver of  
651 auroral motion during a geomagnetic substorm. *Journal of Geophysical Re-*  
652 *search: Space Physics*, *126*, e2020JA029019. doi: [https://doi.org/10.1029/](https://doi.org/10.1029/2020JA029019)  
653 [2020JA029019](https://doi.org/10.1029/2020JA029019)
- 654 Tsyganenko, N. A. (1989). A magnetospheric magnetic field model with the warped  
655 tail current sheet. *Planetary and Space Science*, *37*, 5–20. doi: [https://doi.org/](https://doi.org/10.1016/0032-0633(89)90066-4)  
656 [10.1016/0032-0633\(89\)90066-4](https://doi.org/10.1016/0032-0633(89)90066-4)

- 657 Ukhorskiy, A. Y., Sitnov, M. I., Merkin, V. G., Gkioulidou, M., & Mitchell, D. G.  
658 (2017). Ion acceleration at dipolarization fronts in the inner magneto-  
659 sphere. *Journal of Geophysical Research: Space Physics*, *122*, 3040–3054.  
660 doi: <https://doi.org/10.1002/2016JA023304>
- 661 Wygant, J. R., Bonnell, J. W., Goetz, K., Ergun, R. E., Mozer, F. S., Bale, S. D.,  
662 et al. (2013). The Electric Field and Waves instruments on the Radiation  
663 Belt Storm Probes mission. *Space Science Reviews*, *179*, 183–220. doi:  
664 <https://doi.org/10.1007/s11214-013-0013-7>
- 665 Zhou, X.-Z., Angelopoulos, V., Liu, J., Runov, A., & Li, S.-S. (2014). On the origin  
666 of pressure and magnetic perturbations ahead of dipolarization fronts. *Journal*  
667 *of Geophysical Research: Space Physics*, *119*, 211–220. doi: <https://doi.org/10>  
668 [.1002/2013JA019394](https://doi.org/10.1002/2013JA019394)
- 669 Zhou, X.-Z., Angelopoulos, V., Sergeev, V. A., & Runov, A. (2011). On the nature  
670 of precursor flows upstream of advancing dipolarization fronts. *Journal of Geo-*  
671 *physical Research*, *116*, A03222. doi: <https://doi.org/10.1029/2010JA016165>

# Supporting Information for ”Dipolarization Events With Inductive, Radial Electric Fields Observed by Van Allen Probes”

H. Matsui<sup>1</sup>, R. B. Torbert<sup>1</sup>, H. E. Spence<sup>1</sup>, M. B. Cooper<sup>2</sup>, C. J. Farrugia<sup>1</sup>,

M. Gkioulidou<sup>3</sup>, T. J. Metivier<sup>1</sup>, and J. R. Wygant<sup>4</sup>

<sup>1</sup>Space Science Center, University of New Hampshire, Durham, NH, USA

<sup>2</sup>Center for Solar-Terrestrial Research, New Jersey Institute of Technology, Newark, NJ, USA

<sup>3</sup>The Johns Hopkins University Applied Physics Laboratory, Laurel, MD, USA

<sup>4</sup>School of Physics and Astronomy, University of Minnesota, Minneapolis, MN, USA

## Contents of this file

1. Table S1

**Introduction** This supporting information provides a table of dipolarization events analyzed in this study.

---

**Table S1.** Dipolarization Events Observed by Van Allen Probes and Analyzed in This Study

Probe	Date	Time <sup>a</sup>	Time <sup>b</sup>	Time <sup>c</sup>	$L^d$	MLT <sup>e</sup>	MLAT <sup>f</sup>
B	2013-05-19	07:45:11	07:45:49	07:48:33	5.5	21.4	7.8
A	2013-06-24	00:39:07	00:40:21	00:43:51	6.3	22.0	18.3
A	2013-07-19	18:02:32	18:03:58	18:07:40	5.5	19.4	9.5
B	2015-01-04	16:47:06	16:48:56	16:50:56	4.1	22.0	-9.3
A	2015-01-04	22:37:29	22:37:54	22:42:57	5.5	23.4	-5.8
B	2015-02-01	23:38:23	23:39:07	23:41:16	5.6	22.3	-3.2
A	2015-02-01	23:39:18	23:39:54	23:40:41	5.4	22.2	-3.2
A	2015-02-01	23:46:36	23:47:52	23:49:46	5.4	22.3	-3.3
A	2015-02-02	18:52:36	18:54:39	19:02:15	6.3	23.2	-17.1
B	2015-03-02	06:31:35	06:32:57	06:33:23	5.7	23.0	-2.0
A	2015-03-07	06:34:08	06:36:26	06:44:09	5.4	21.5	-5.3
B	2015-04-16	08:07:58	08:10:23	08:14:06	5.8	20.3	-10.5
A	2015-04-17	02:48:39	02:51:15	02:58:13	5.8	21.4	4.4
B	2015-04-21	04:49:26	04:53:08	04:57:11	5.3	19.7	-4.4
B	2015-06-09	22:49:06	22:50:41	22:54:50	5.9	19.6	10.8
A	2015-06-09	22:49:22	22:52:07	22:54:43	6.0	19.3	11.1
B	2015-07-05	04:59:53	05:02:10	05:06:09	5.2	19.1	9.7
B	2016-12-22	05:38:35	05:39:30	05:42:06	6.2	22.1	13.8
B	2017-04-01	15:04:22	15:05:51	15:12:00	5.7	19.4	-16.2
B	2017-04-20	03:06:36	03:16:20	03:24:18	4.7	19.6	-2.7
B	2018-09-13	11:04:26	11:06:26	11:10:54	5.9	22.7	-7.9
B	2018-09-13	11:30:24	11:31:46	11:34:53	5.9	23.0	-7.5

<sup>a</sup> Beginning of the dip.

<sup>b</sup> Ending of the dip or beginning of the dipolarization front (DF).

<sup>c</sup> Ending of the DF.

<sup>d</sup> Dipole  $L$  Value.

<sup>e</sup> Magnetic Local Time in H.

<sup>f</sup> Magnetic Latitude in Deg.